

COUPLED TWIN CONICAL FUNNELS OR CONICAL HOSES: AN INTERNAL PROCESS OF DYNAMIC FLOW DISTRIBUTION.

RICARDO T. FERREYRA¹

¹Facultad de Ciencias Exactas, Físicas y Naturales. Universidad Nacional de Córdoba
Avenida Velez Sarsfield 1110. CP5000. Córdoba. Argentina
ricardo.tomas.ferreyra@unc.edu.ar. and <https://fcefyn.unc.edu.ar/>

Key words: Shock Waves, Internal Flow, Matter Distribution.

Abstract. The first objective of this study is to revisit an analytical test by the author that helps now for a prediction and explanation for the likely physical existence of twin funnels in the fluid crossed by shock wave, under certain conditions. These funnels function like a conical hose within shock waves traveling through matter. In terms of the laws of continuity, momentum, and energy the classical shock wave model is empowered with a not widespread actual function that explains a nonlocal physical phenomenon of matter distribution. The second objective is the recognition and application of two almost new analytical boundary conditions $V_{1S} = -V_1$ and $M_{1S} = iM_1$, provided in the recent past that open the theory to the, at least, analytical existence of hoses or coupled twin funnels. Finally, given that supersonic and hypersonic solid cones are related to theoretical, experimental, natural, aeronautical, astronautical, geophysical and industrial interests, among others, certain analytical regions derived from this recently characterized formulation are shown and hoses or twin funnels located among them. These regions can be visualized on the plot of cone angle, shock angle, and free-stream Mach number for analogy, comparison, and prediction.

1 INTRODUCTION

At the present time, after the names of Ernst Mach (1838-1916), Busemann (1929), Taylor-Maccoll 1933, Stone (1952), Hayes-Probstein (1966), Anderson (2003), and their remarkable contributions [1-6], it appears it was worthy recent developments for extending analytical Shock Wave model to explain potential unobservable phenomena [7-11], or at least, to predict some real unmeasurable events at the time they are happening [12-15]. So, two issues motivated this work: First, a new Shock Wave Front model, named SWF model, developed to extend the classical Shock Wave model, named SW model, because the novel SWF model was needed to deeply connect the Shock Wave phenomena with the new associated formulation and predicted phenomena. Second, the recent development of the equations $V_{1S} = -V_1$ and $M_{1S} = iM_1$, a pair of two almost new boundary conditions inside the SW, had to be well founded by using Fluid Mechanics Laws [7-11]. To begin, let us keep in mind what was

considered the classical model of a Shock Wave, SW model. In Fig. 1, the classical SW model is presented satisfying mass, momentum, and energy equations.

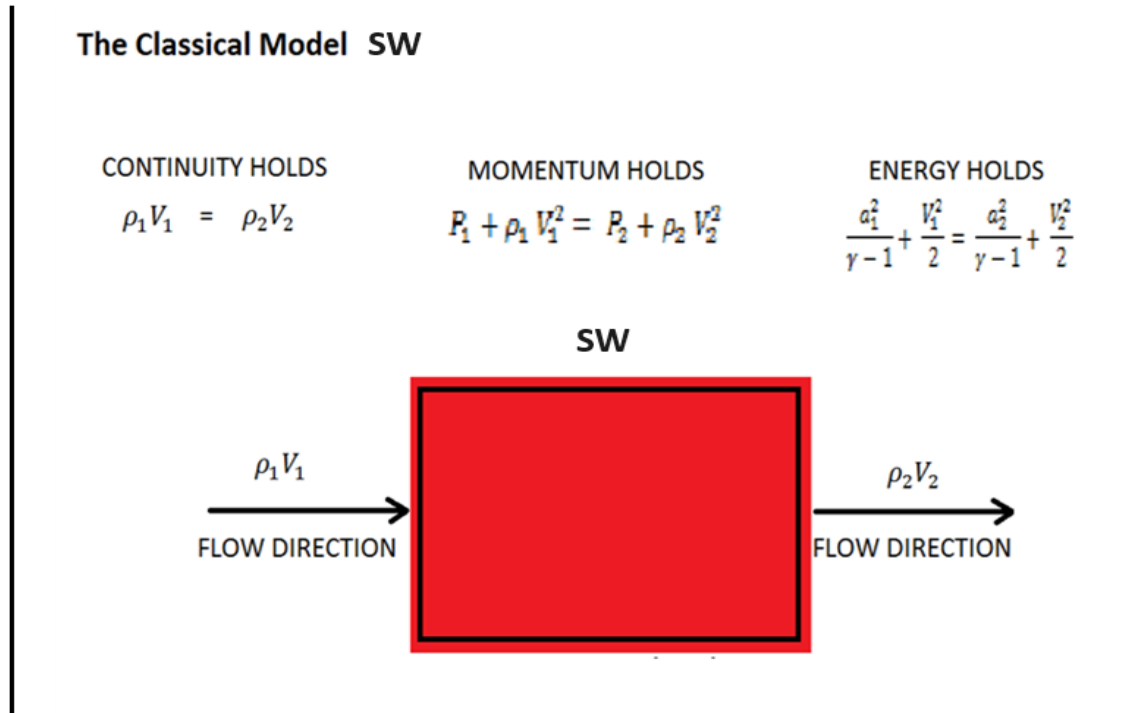


Figure 1: The SW Classical model. The Mass, Momentum and the Energy Conservation along the horizontal direction or flow direction in the Classical model.

In Fig. 2, the nonclassical model is presented. A Shock Wave Front had been included in the middle of the SW classical model to obtain the new SWF model. At the Shock Wave Front, SWF, the Mach number M_1 has another important meaning related to the mass and energy distribution that was written as $M_{1S} = iM_1$, where i represents the imaginary unit [8,9]. Also, at the shock wave front (upstream), the free stream velocity is $V_{1S} = -V_1$. The proof of these equations derived from the physical laws was the main goal of that works. Although in Fig. 1, the conservation Laws of Mass, Momentum and Energy hold between two external points to SW (in Fig. 1, the SWF was ignored), a vertical thick line representing the Shock Wave Front SWF was added in Fig. 2 (here, the SWF was considered) in order generate a new internal place inside SW where $V_{1S} = -V_1$ and $M_{1S} = iM_1$ take place. This new place is named the SWF.

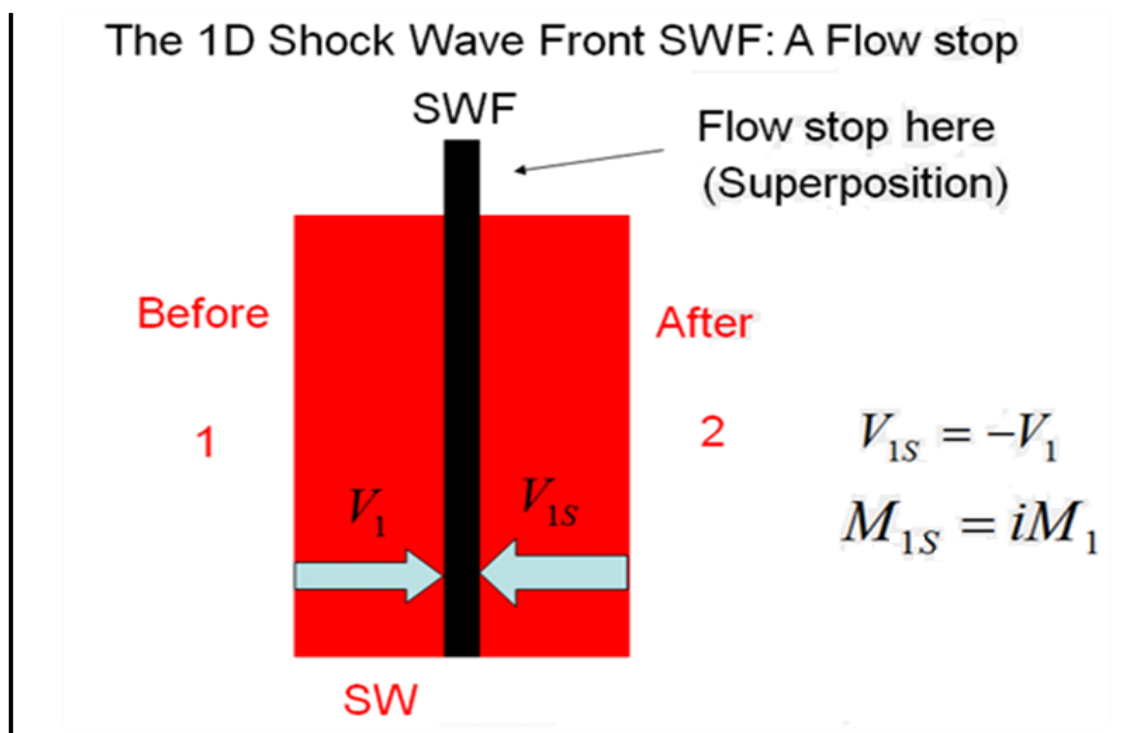


Figure 2. The SWF model: As a first step, a vertical thick line is assumed in any place into the SW model (SW is the classical model) to derive after few steps, the SWF model.

Since $V_{1S} = -V_1$ over the SWF, it is difficult for the flow not to collide. The flow is coming from both sides, see Fig. 2, to hold the original direction. The left side is quiet and the flow from the right is travelling to the left and colliding with velocity V_{1S} or, on the other hand, the right side is quiet and the flow from the left is traveling to the right and colliding with velocity V_1 . So, whatever happens, the concept of one-dimensional flow is considered in Fig.2 neither physical nor realistic. This procedure allows developed the proof for the SWF model, which was proposed, analyzed, and founded throughout the Laws of Mass, Momentum and Energy conservation in both directions (real and imaginary). Thus, these Laws hold not only along the flow direction (horizontal direction), but also in the Shock Wave direction (vertical direction). In 2016, the Shock Wave Front model was early presented after its effectiveness in analyzing new theoretical boundaries [11], but in 2018 and 2020, the Fluid Dynamics Laws were needed and applied to provide a more formal proof for the analytical validity of the SWF model, after the universality of the Physical Laws.

For the better lecture of what follows, Table 1 is for nomenclature.

Table 1: Nomenclature.

Symbol	Meaning
$[\]_1$	= property evaluated before the wave
$[\]_2$	= property evaluated after the wave
$[\]_s$	= property evaluated at the shock wave front
$[\]_b$	= property evaluated at the shock wave back
M_1	= Mach number of the free flow (dimensionless)
M_{1s}	= Mach number at the shock wave front (dimensionless)
θ_c	= solid cone semi-angle (radians)
θ_s	= shock wave semi-angle (radians)
θ	= spherical coordinate, azimuth angle (radians)
V_{Lim}	= highest dimensional velocity that the h_0 enthalpy flow can reach (m / s)
V_R	= component of velocity in the radial direction (dimensionless)
V_θ	= component of velocity in the tangential direction
$V_{\theta\theta}$	= derivative of tangential velocity with θ as variable (dimensionless)
V_I	= velocity of the free flow (dimensionless)
C_p, C_v	= specific heats at constant pressure and at constant volume (J / (kg K))
γ	= ratio of specific heats, C_p/C_v (dimensionless)
a	= velocity of sound, m / s.
ρ	= density function, kg / m ³ .
P	= pressure function, N / m ² .
q	= rate of heat added per unit of mass, J / kg
f	= body force per unit of area, N / m ² .
S	= entropy function, J / °K.

3 APPLICATION OF THE SWF MODEL

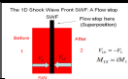
There is a genuine interest of analyzing transitions to hyper velocities, also to understand processes of a supersonic solid cone that becomes thinner, or thicker, or just changes its size during its movement inside a compressible flow and, also to predict or explain complex phenomena in related matter. In general, but in simple terms, one state of matter is a limiting case of the others. For example, one can think that a solid is a limiting case of liquid or gas. One can also predict that inside a complex limiting process what really matters is mass, momentum and energy balance, whatever state it is having the matter at the time of analysis. Like this one, similar practical ideas are of interest. In this sense, here, the classical equation of Taylor-Maccoll is just a starting point for the following derivations.

3.1 Explicit Formulation for θ_c in the form $\theta_c = \theta_c(M_1, \theta_s)$

Table 2 helps to know how the SWF model is applied to the $V_\theta(\theta_s)$ boundary condition of the Taylor and Maccoll problem and then for obtaining an explicit formulation for θ_c . The point

1_S is adopted to refer the SWF location. As an example, the procedure is shown for $(\theta_S - \theta_C \rightarrow 0)$,

Table 2: Explicit Formulation for θ_C

Step	Explanation	The SWF model is applied.
1	SWF Model	
2	Boundary Condition of the Taylor–Maccoll Problem	$\frac{V_\theta(\theta_S)}{-V_{1S} \sin(\theta_S)} = \frac{1}{\left(\frac{\gamma+1}{2}\right)} \left[\left(\frac{\gamma-1}{2}\right) + \frac{1}{M_{1S}^2 \sin^2(\theta_S)} \right]$
3	$V_{1S} = -V_1$	$\frac{V_\theta(\theta_S)}{V_1 \sin(\theta_S)} = \frac{1}{\left(\frac{\gamma+1}{2}\right)} \left[\left(\frac{\gamma-1}{2}\right) + \frac{1}{M_{1S}^2 \sin^2(\theta_S)} \right]$
4	$M_{1S} = iM_1$	$\frac{V_\theta(\theta_S)}{V_1 \sin(\theta_S)} = \frac{1}{\left(\frac{\gamma+1}{2}\right)} \left[\left(\frac{\gamma-1}{2}\right) - \frac{1}{M_1^2 \sin^2(\theta_S)} \right]$
5	Solving for $V_\theta(\theta_S)$	$V_\theta(\theta_S) = \frac{V_1 \sin(\theta_S)}{\left(\frac{\gamma+1}{2}\right)} \left[\left(\frac{\gamma-1}{2}\right) - \frac{1}{M_1^2 \sin^2(\theta_S)} \right]$
6	Considering $V_\theta(\theta_S)$ for the case $(\theta_S - \theta_C \rightarrow 0)$	$\begin{aligned} -\sqrt{2} \left[\frac{V_1 \cos(\theta_S)}{\cos(\theta_S - \theta_C)} \right] \sin[\sqrt{2}(\theta_S - \theta_C)] \\ = \frac{V_1 \sin(\theta_S)}{\left(\frac{\gamma+1}{2}\right)} \left[\left(\frac{\gamma-1}{2}\right) - \frac{1}{M_1^2 \sin^2(\theta_S)} \right] \end{aligned}$
7	Solving for θ_C	$\theta_C = \theta_S - \frac{1}{\sqrt{2}} \arctan \left(\frac{\tan(\theta_S)}{\sqrt{2} \left(\frac{\gamma+1}{2}\right)} \left[\frac{1}{M_1^2 \sin^2(\theta_S)} - \left(\frac{\gamma-1}{2}\right) \right] \right)$

3.2

Transitions to conical hoses or coupled twin conical funnels: Characterization of four regions and the limiting curve $\theta_C = \theta_S$

In Fig. 3, four new regions and its upper boundaries were found. The four upper boundaries are associated with hypersonic flow, higher supersonic flow, lower supersonic flow and the last is related to transonic or subsonic flow. The curve $\theta_C = \theta_S$ is an unrealistic upper limit condition in the $(\theta_C, \theta_S, M_1)$ chart. However, Figure 3 shows that higher cone angles cannot reach higher Mach numbers and the limiting Mach number condition occurs over $\theta_C = \theta_S$ for both supersonic and hypersonic flow.

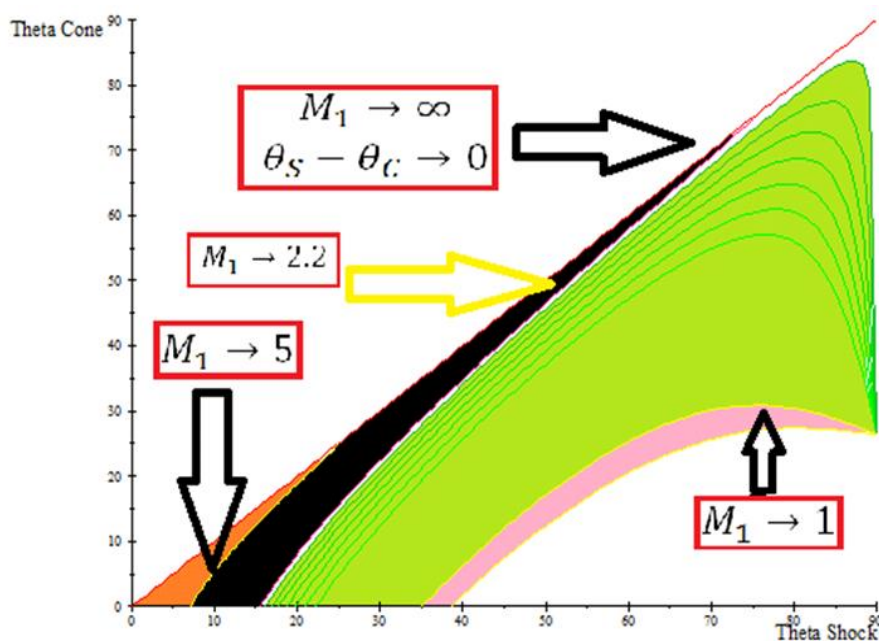


Figure 3: SWF model. Under $(\theta_S - \theta_C \rightarrow 0) : \theta_C = \theta_C(\theta_S, M_1)$ at different Mach numbers.

The first region is the region associated with hypersonic flow $M_1 \geq 5$ after the SWF model, but only thin cones, namely $\theta_C \leq 25^\circ$, can access to this hypersonic velocity condition at the time that hold the same pattern of the physical phenomena (attached Shock Wave SW and zero angle of attack in the Taylor-Maccoll problem). The value of $\theta_C \approx 25^\circ$ is a horizontal line where thin cones start being thick. On the left sector of the chart, over this line, $\theta_C \approx 25^\circ$, there is a point where both thick and thin cones share the highest theoretical value of $\theta_S \approx 25^\circ$ for hypervelocity regime. One can check this point happens for $M_1 = 5$ and $\theta_C \approx 25^\circ$. Now, see the chart on the left, where hypersonic region begins from a short horizontal segment between beginning on the origin of the reference system, namely point $\theta_C = 0^\circ$ and $\theta_S = 0^\circ$ and the point $\theta_C = 0^\circ$ and $\theta_S \approx 8^\circ$ over the horizontal axis, more to the right. Above this short horizontal segment, the hypervelocity region spreads. The second region is bounded by the curves for the Mach numbers of $M_1 = 2.2$ until $M_1 = 5$. So, this second region is the upper supersonic region. Due to dimensional consequences derived from the SWF model, the distribution of matter and energy also occurs in the Shock Wave direction. In fact, the phenomenon of matter distribution by hoses in this region can be generated. The phenomenon always exists here, analytically. This is because: 1) the region of hoses is under the physical limit $\theta_C = \theta_S$, 2) it involves higher θ_C values where it is not possible hypervelocity, 3) this region of hoses is below the region of very thick cones where a physical relation among θ_S and θ_C is full predictable, and finally, 4) the region of hoses is above the superior limit of the classical theory for one dimensional supersonic flow, as it can be seen in the next section, where only one dimensional phenomena takes place. So, the two-dimensional movement through

hoses is possible after it satisfies the mass, momentum, and energy conservation laws. The third region is bounded by the Mach numbers of $M_1 = 1$ until $M_1 = 2,2$ and is the lower supersonic region. Again, the value of $\theta_c \approx 25^\circ$ is a horizontal line where thin cones start being thick. This horizontal line is, theoretically, the place in the chart where thin cones change to thick cones in crossing this line throughout a vertical path from a lower θ_c to a higher θ_c . Figure 3 also shows that lower supersonic flow, that is to say $1 \leq M_1 \leq 2,2$, is allowed for almost all cone angles. On the right sector of the chart, the limit for these curves that satisfies $1 \leq M_1 \leq 2,2$, is a point. These two regions are the lower supersonic. The transonic region and the lower supersonic regions together have a common limit point on the right. The limit point on the right is theoretically associated with a Shock Wave angle of $\theta_s = 90^\circ$ and a cone angle of $\theta_c \approx 25^\circ$. Until now, we have described under SWF model, three supersonic regions.

The fourth region according to SWF is transonic or subsonic and every point in this region satisfies $M_1 \leq 1$. In the SWF model, notice that for the first, third and the fourth regions an horizontal line crosses every curve twice in the chart $(\theta_c, \theta_s, M_1)$, which means that for every θ_c on the vertical axis there are two possible values of θ_s for a given Mach number. This fact does not happen in the hoses or twin funnels region (the second region) because here even the SWF, the closer we have, does not work. Complementarily, this fact happens whenever this horizontal line does not touch the lowest boundary curve of the fourth region, where below this lowest curve this behavior does not happen anymore in this transition to transonic region. So, this is the last horizontal line in the chart with this behavior. The formulation for $(\theta_s - \theta_c \rightarrow 0)$ obtained from the SWF model generates different regions. In the supersonic case, it means regions for very thick cones, for hypervelocity or just regions where transitions to “conical hoses” or “twin funnels” are theoretically validated to take place. The Fig. 3 deals with only the SWF model. In Table 2 was explained how the formulation for θ_c is derived for very thick cones whether the SWF model is applied. The Fig. 4 deals with both SWF and SW models. In Table 3, the limit $(\theta_s - \theta_c \rightarrow 0)$ opens many perspectives. At least the possibility of hypervelocity or the possibility of thick cones are considered, but also the θ_c formulations for both cases the SWF model and the SW model are shown. After these formulations in Fig. 4, six regions are obtained and characterized, but the focus takes place only over those regions that lay over the upper limit line $\theta_s = \theta_c$, which are only three regions of the six regions. In Fig. 4, the line $M_1 \rightarrow \infty$ of the SW model is applied as a reference line due to the fact that over this line only the SWF model can be applied and SW model cannot. Below this line, both SWF and SW can be applied. For instance, the SW model can be taken into account to draw the chart, only whenever $\theta_s \geq 25^\circ$. So, in order to analyze upper regions associated with the SWF model, the focus is above the line $M_1 \rightarrow \infty$ of the SW model or above the line $M_1 = 5$ of the SWF model, but always below the upper limit line $\theta_s = \theta_c$ which is derived analytically by the new SWF model. Now, for comparison purposes, both the SWF and the SW models are analyzed. Table 3 provides the θ_c formulations for the wide condition $(\theta_s - \theta_c \rightarrow 0)$, but considering two different circumstances: 1) the SWF model is applied (The point 15 is adopted in SWF), and

2) SWF is not applied, but SW (The point 1 is adopted in SW). Note that θ_c for the case 1) is derived from SWF model. To this end, the cone angle versus the Shock angle for different Mach numbers are shown in Fig. 4. The SWF model generates three new regions little below the condition $\theta_s = \theta_c$, but above the curve $M_1 \rightarrow \infty$ of the SW. One for very thick cones, in the sense of $V_\theta \rightarrow 0$. Other for hypersonic flow, $M_1 > 5$ of the SWF. And another region for conical hoses or twin funnels, between them. However, SWF and SW comparison implies more details. For instance, note or recall that $M_1 \rightarrow \infty$ implies one curve for SWF and one curve for SW. The same occurs with other conditions. Naturally, under the curve $M_1 \rightarrow \infty$ of the SW, other regions are generated or derived from the analytical comparison between SWF and SW. Three of them are illustrated in the chart of solid cone semi-angle as a function of the Shock Wave semi-angle for different Mach numbers. In this study, it is suspected that novelty was generated after the equations $V_{1s} = -V_1$ and $M_{1s} = iM_1$, a pair of two recent boundary conditions from Fluid Mechanics Laws [7-11]. So, now, let us focus on new regions above the curve $M_1 \rightarrow \infty$ of the SW.

Table 3: A comparison between WS and SWF for obtaining θ_c

A comparison between SW and SWF for θ_c		
1	SWF Model	$\theta_c = \theta_s - \frac{1}{\sqrt{2}} \arctan \left(\frac{\tan(\theta_s)}{\sqrt{2} \left(\frac{\gamma+1}{2} \right)} \left[\frac{1}{M_1^2 \sin^2(\theta_s)} - \left(\frac{\gamma-1}{2} \right) \right] \right)$
2	SW Model	$\theta_c = \theta_s - \frac{1}{\sqrt{2}} \arctan \left(\frac{\tan(\theta_s)}{\sqrt{2} \left(\frac{\gamma+1}{2} \right)} \left[\frac{1}{M_1^2 \sin^2(\theta_s)} + \left(\frac{\gamma-1}{2} \right) \right] \right)$

Coming from the right to the left, the first new region is above the curve $M_1 \rightarrow \infty$ of the classic SW model in the $(\theta_c, \theta_s, M_1)$ chart, where we have very thick supersonic cones whenever $M_1 \leq 2.2$. This region is derived from the SWF model, but it is not allowed for the SW classical model because it is above of its upper limit. The second new region is a very thin dual region (in this case it is supersonic from the SWF model, and it is not allowed from the SW model). This region touches the line $\theta_s = \theta_c$ along the range $20^\circ \leq \theta_s \leq 75^\circ$. In fact, since this region is below $M_1 = 5$ of the SWF model, it is supersonic, but it is banned for the SW model since it is above its upper limit, which is the curve $M_1 \rightarrow \infty$ for the SW model. More specifically, this region is the thinner of the three regions above the curve $M_1 \rightarrow \infty$ for the SW

model. According to what was explained in section 3.2 this part of the region of hoses or twin funnels. The third, and the last new region, is placed at the left bottom of the chart in Fig. 4. To be on the left, this region satisfies $\theta_s \leq 25^\circ$. Also, this region is above the curve $M_1 = 5$ of the SWF model and below the line $\theta_s = \theta_c$. Here, we have that both the SWF model and the SW model agree in considering this region as a hypersonic one. Finally, note that these three new regions have quite different shapes.

Also, note that these three mentioned regions are only generated from the SWF analytic model. However, as mentioned before, there are other regions, but they are out of the focus of this analysis. This is because these other ones are below the curve $M_1 \rightarrow \infty$ for the SW model and, consequently, they belong to both the SWF and SW models. So, they are out of the focus of this study since they can also be obtained throughout the classic SW model as a set of well-known lower references in the region. However, even three of them are in Fig. 4.

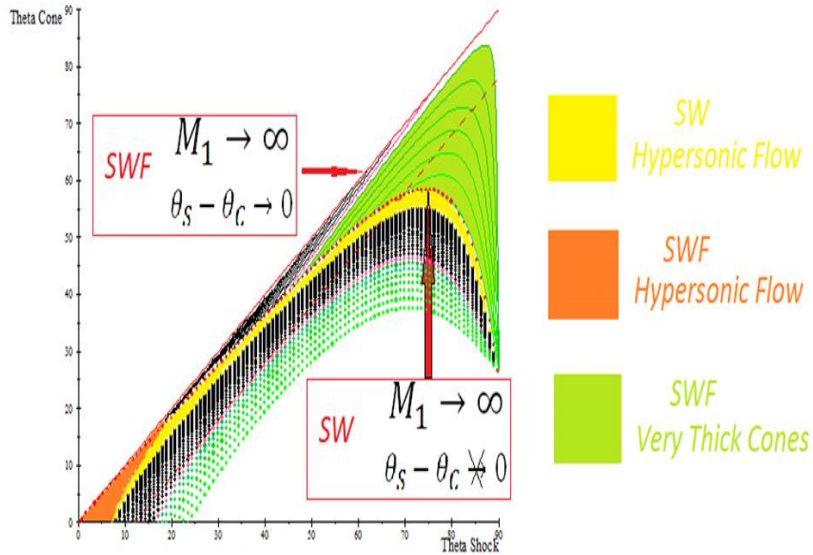


Figure 4: New regions from the SWF and SW comparison in the $(\theta_c, \theta_s, M_1)$ chart.

From above to below, the first one below the curve $M_1 \rightarrow \infty$ for the SW model is between the curves $M_1 \rightarrow \infty$ and $M_1 = 5$ for the SW model. This is a very thin region below the curve $M_1 = 5$ of the SWF model and above the curve $M_1 = 5$ for the SW model. So, it is supersonic from the SWF model point of view, but it is hypersonic from the SW model perspective. This dual behavior is extended along all range of θ_s . The dual behavior is not a real problem since it comes from the incompleteness of the classical SW model. The second region out of the focus is supersonic $1 \leq M_1 \leq 5$ and the third one is just subsonic. Note that, see Fig. 4, these three regions are the same-shaped three regions in the lower part of the chart $(\theta_c, \theta_s, M_1)$.

Now, revisit hoses region. Let us go again above the curve $M_1 \rightarrow \infty$ for the SW model and below the curve $\theta_s = \theta_c$ for SWF model, and between hypersonic flow region and very thick cones region. From one side, hypersonic flow cannot happen “easily” for higher θ_c values. From the other side, higher θ_c values cannot reach “easily” hypersonic velocities without distribution of matter. So, the more accentuated and preserved geometrical transition to conical hoses is derived from the SWF-SWB or SWF models proposed in the literature [7-11]. In section, 3.2, the hoses region was characterized and bounded by the curves for $M_1 = 2.2$ and $M_1 = 5$ among the other two mentioned regions (hypersonic and thick cones regions). In this case, we deal with an upper supersonic region. Then, after dimensional consequences together with the SWF model and combined with the physical laws of conservation, the matter distribution is predicted in the direction of the Shock Wave, internally, between the Shock Wave Front SWF and the Shock Wave Back SWB, [10,11].

To summarize:

If:

- 1) the region of hoses is under the physical limit $\theta_c = \theta_s$,
- 2) the region of hoses involves θ_c values that are above the θ_c values of the hypervelocity region,
- 3) the region of hoses involves θ_c values that are below the θ_c values of the region of very thick cones, where a physical relation among θ_s and θ_c is full predictable,
- 3) in applying the SWF model, a horizontal line does not cross every curve twice in the chart $(\theta_c, \theta_s, M_1)$, This fact does happen in the hoses or twin funnels region. The hoses region is the only with this property below the $\theta_c = \theta_s$ curve.
- 4) the region of hoses is above the superior limit of the classical theory for one dimensional supersonic flow, incomplete but fully accepted SW theory as it was explained in section 3.3, where only one-dimensional phenomena take place. That is to say, the region of hoses is above the curve $M_1 \rightarrow \infty$ for the classical SW model, and finally,
- 5) this region of hoses allows at least two-dimensional movement that satisfies the mass, momentum, and energy conservation laws.

Then:

- a) two-dimensional flow distribution phenomenon exists in 2D flow, and
- b) an axisymmetric flow distribution (matter distribution) by hoses or twin funnels exists in 3D flow.

5 CONCLUSIONS

The boundary conditions $M_{1s} = iM_1$, and $V_{1s} = -V_1$, after the Shock Wave Front model, and Mass, Momentum and Energy conservation from the field of Fluid Mechanics allow us to conclude in the existence of a near axisymmetric flow distribution (matter distribution) by hoses

or twin funnels in 3D flow under certain physical conditions. In addition, the SWF model was applied to formulations for very thick cones, and four new regions were characterized. Then, a comparison between new regions that has been derived from the SWF model and those classical who has not, shows that the SWF model provides new more realistic boundaries in the local analysis, but in the global. Applications in supersonic cones allows us to find analytical hoses or twin funnels that potentially helps the prediction of internal matter or energy distribution. Finally, these results are of practical interest since the limit regions for cones has applications in industry and the new boundaries that define regions helps in predictions related to compressible flow and helps in building new necessary theoretical support.

REFERENCES

- [1] Busemann, A. Druke auf Kegelförmige Spitzen bei Bewegung mit Überschallgeschwindigkeit. *Zeitschrift für Angewandte Mathematik und Mechanik*. (1929) **9**: 496-498.
- [2] Taylor, G. I. and Maccoll, J. W. The air pressure on a cone moving at high speeds. *Proceedings of the Royal Society of London, Series A*. (1933) **139-(838)**: 278-297.
- [3] Stone, A. H. On supersonic flow past a slightly yawing cone. *Journal of Mathematical Physics*. (1948) **27**: 67-81.
- [4] Stone, A. H. On Supersonic Flow Past a Slightly Yawing Cone. *Journal of Mathematical Physics*. (1952) **30**: 220-223.
- [5] Hayes, W. D. and Probstein, R. F. *Hypersonic flow theory*. Academic Press., New York, 2nd edition, (1966).
- [6] Anderson, J. D. *Modern Compressible Flow with Historical Perspective*. Mc Graw Hill, Series in Aeronautical and Aerospace Engineering, 3rd edition, New York, (2003).
- [7] Ferreyra, R. T. and Tamagno, J. P. A non-local technique to approach the solutions of nonlinear boundary value problems applied to a supersonic flow model. *International IFNA-ANS Scientific Journal Problems of Nonlinear Analysis in Engineering Systems, PNAES*. (2012) **18-(2)-(38)**: 48-63.
- [8] Ferreyra, R. T. An infinite number of closed form solutions for the Taylor and Maccoll Problem. *International IFNA-ANS scientific Journal Problems of nonlinear analysis in engineering systems, PNAES*. (2014) **20-(2)-(42)**: 52-59.
- [9] Ferreyra, R. T. New Tools and results in the study of a supersonic flow over a solid cone. *International IFNA-ANS Scientific Journal Problems of Nonlinear Analysis in Engineering Systems, PNAES*. (2015) **21-(43)**: 93-106.
- [10] Ferreyra, R.T. Supersonic Needles at Zero Incidence. *AIAA American Institute of Aeronautics and Astronautics, 46th AIAA Fluid Dynamic Conference, AIAA Aviation* (AIAA 2016-4275). URL: <http://dx.doi.org/10.2514/6.2016-4275> [cited 28 October 2016].
- [11] Ferreyra, R. T., A Shock Wave Front Model Applied to Very Thick and Very Thin Supersonic Cones at Zero Incidence. *American Institute of Aeronautics and Astronautics. 8th AIAA Theoretical Fluid Mechanics Conference, AIAA AVIATION Forum, (AIAA 2017-3347)*. <https://doi.org/10.2514/6.2017-3347>

- [12] Ivanov B. A., Bazilevskiy A. T., Sazonova L. V. *Meteoritika. Akademiya nauk SSSR, Nro 40, 1982, pp 67-81, Translation Nasa Technical Memorandum, TM-88427, (1982).*
- [13] Ferreyra R. T., Shpekin M. I. A fluid dynamical model to shape complex craters XXXIV Intern. Conf. on Interaction of Intense Energy Fluxes with Matter (EOS-2019) Book of Abstracts, Moscow & Chernogolovka & Nalchik, March 1-6, (2019) 397 pages. ISBN 978-5-6040595-9-3.
- [14] Ferreyra R. T., Shpekin M. I. A likely dynamical balance for complex crater formation XXXV Intern. Conf. Equation of State for Matter (EOS-2020) 14p. (in print).
- [15] Shpekin M. I. and Ferreyra R.T. Estimation of the state of matter in young impact craters on the Moon based on the orbital observations. *15th World Congress on Computational Mechanics (WCCM-XV) 8th Asian Pacific Congress on Computational Mechanics. (APCOM-VIII) S. Koshizuka (Ed.), Volume 600 Fluid Dynamics and Transport Phenomena, 2022, DOI: 10.23967/wccm-apcom.2022.047*